ChemComm

Accepted Manuscript

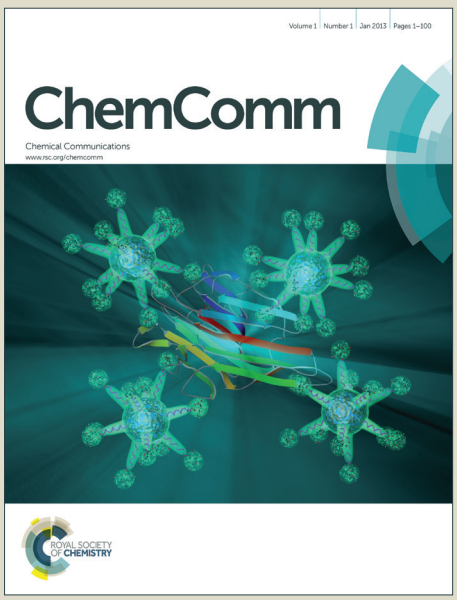

ROYAL SOCIETY OF CHEMISTRY

www.rsc.org/chemcomm

Journal Name

COMMUNICATION

Hexangular ring-core $NiCo_2O_4$ porous nanosheet/NiO nanoparticle composite as advanced anode material for LIBs and catalyst for CO oxidation applications

Received 00th January 20xx,
Accepted 00th January 20xx

DOI: 10.1039/x0xx00000x

www.rsc.org/

Yanyan He, Liqiang Xu*, Yanjun Zhai, Aihua Li and Xiaoxia Chen

Porous hexangular ring-core $NiCo_2O_4$ nanosheet/NiO nanoparticle composite has been synthesized by a hydrothermal method followed an annealing process in air. The as-obtained composite as anode material exhibits a high initial discharge capacity of 1920.6 mA h g^{-1} at a current density of 100 mA g^{-1} and the capacity is retained at 1567.3 mA h g^{-1} after 50 cycles. When it is utilized as catalysts for CO oxidation, the complete CO conversion is achieved at 115 □ and the catalytic life test demonstrates the good stability of the composite.

In recent years, Lithium-ion rechargeable batteries (LIBs) have become one of the most important power sources of portable electronic devices because of their high energy density and high voltage. Much effort have been concentrated on anode materials especially transition metal oxides, such as Co_3O_4, [1] NiO,[2] Fe_2O_3, [3] have drawn great concern due to their high theoretical specific capacities. For example, Co_3O_4 shows almost the highest capacity among them (theoretical capacity: 890 mA h g^{-1}). The capacity of porous Co_3O_4 nanocages maintained at 1465 mA h g^{-1} after 50 cycles at a current density of 300 mA g^{-1}.[4] Meanwhile, Co_3O_4 has been one of the most promising catalysts for CO oxidation in room temperature even at low temperature.[5] However, Co_3O_4 cannot be perfect candidate as anode material or catalyst for CO oxidation due to its toxicity and high cost, therefore，it is necessary to explore cheaper and eco-friendly alternative metals replace Co_3O_4 partially, such as $NiCo_2O_4$,[6] $CuCo_2O_4$[7] and $MnCo_2O_4$[8] materials, which are all isostructural to Co_3O_4.

Among these materials mentioned above, $NiCo_2O_4$ has almost the same capacity (theoretical capacity: 884 mA h g^{-1}) to Co_3O_4 and improved electrical conductivity (Co_3O_4: 3.1×10^{-5} S cm^{-1}, $Ni_xCo_{3-x}O_4$:0.1-3 S cm^{-1}). [9] Meanwhile, it has easy electrolyte penetration and low diffusion resistance ability to cations. [10] On accounting of these advantages compared with Co_3O_4, $NiCo_2O_4$ material has been considered as promising anode material for LIBs. In addition, it has been utilized as catalyst for CO oxidation and as excellent selectivity and high sensitivity to various gases such as ethanol and SO_2 [11]. Up to now, there are two reports about $NiCo_2O_4$ as catalyst for CO oxidation. [12, 13] However, the large volume changes and aggregation during discharge/charge processes caused the poor stability of $NiCo_2O_4$ material. Besides $NiCo_2O_4$, NiO material (theoretical capacity is 718 mA h g^{-1}) has lower cost, higher natural abundance and more friendly to the environment than Co_3O_4 and $NiCo_2O_4$, but it has poor electrical conductivity. As we all know, electrochemical performance of LIBs highly depends on the structure of the electrode materials, including morphologies, sizes and the conditions of surface and so on. Accordingly, it is necessary to exploit $NiCo_2O_4$ with novel stable nanostructure or build $NiCo_2O_4$ nanocomposite with other suitable materials.

Hexangular ring or ring-core structured materials, such as $CuFeO_2$ hexagonal platelets/rings, [14] Ni $(OH)_2$@$Co(OH)_2$ hollow nanohexagons [15] have been reported and the results showed the better electrochemical performance than those of common morphologies. Ring-core structured materials own uniform hexangular size and large surface area due to the inner core and hexagonal ring, they are favourable to effectively buffer the volume changes and aggregation of particles during discharge/charge processes. Therefore, it is feasible to design and fabricate similar structured $NiCo_2O_4$ to enhance electrochemical performance. In addition, $NiCo_2O_4$ nanocomposite has been studied widely and the result showed that the synergistic effect between $NiCo_2O_4$ and another material effectively improved the performance. For instance, $NiCo_2O_4$/RGO nanosheet composite materials show a reversible capacity of 816 mAhg^{-1} after 70 cycles at a current density of 100 mA g^{-1},[16] $NiCo_2O_4/Fe_2O_3$ porous nanocages exhibit a reversible capacity of 1079.6 mA h g^{-1} after 100 cycles at a current density of 100 mA g^{-1}.[10] Nevertheless, the electrochemical performances of all these $NiCo_2O_4$ materials especially their capacity retention and cycling stability are far away from satisfaction.

In this study, hexangular ring-core porous $NiCo_2O_4$ nanosheet /NiO nanoparticle composite has been synthesized through a facile hydrothermal process followed an annealing process in air. As far as we know, $NiCo_2O_4$ material with similar core-ring structure has been applied in the fields of electrocatalysis[17] and photocatalysis[18]. However, to the best of our investigation, $NiCo_2O_4$ material with unique ring-core structure has not been applied as anode electrode material for LIBs and catalyst for CO oxidation. As an anode material for LIBs, the ring-core $NiCo_2O_4$/NiO composite delivered the initial discharge capacity of 1920.6 mA h g^{-1} and the specific capacity could be maintained at 1567.3 mA h g^{-1} after 50 cycles at a current density of 100 mA g^{-1}, much higher than those in previous reports (see Table S1). In addition, the comparisons between the $NiCo_2O_4$/NiO composite and previously reported anode materials are shown in Table S2, indicating obvious advantages in capacity and cycle life of the composite has been achieved. On the other hand, the CO oxidation catalytic activities indicated that complete CO conversion was achieved at 115 □, the catalysts demonstrated good stability with almost no changes relative in the 75% CO conversion after 120 min on stream and the temperatures for the catalytic life tests was 108 □, respectively. According to its enhanced performance, the $NiCo_2O_4$/NiO composite has great promise for its

widely potential applications in anode material for LIBs and catalyst for CO oxidation in the future.

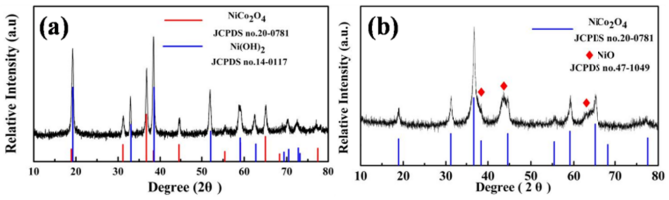

Fig. 1 XRD patterns of (a) the product obtained after the hydrothermal reaction; (b) the products after the calcinations (350 ℃).

Fig. 1 (a) shows the XRD pattern of the product obtained after the hydrothermal reaction and all the diffraction peaks could be indexed to hexagonal $Ni(OH)_2$ (JCPDS card no.14-0117) and cubic $NiCo_2O_4$ (JCPDS card no.20-0781). As shown in Fig. 1 (b), the cubic $NiCo_2O_4$ (JCPDS card no.20-0781) and cubic NiO (JCPDS card no.47-1049) are co-existed in the products after the calcinations process of 350 ℃.

The morphologies of $NiCo_2O_4$ nanosheet/$Ni(OH)_2$ nanoparticle composite and the hexangular ring-core $NiCo_2O_4$ porous nanosheet/NiO nanoparticle composite (350℃) are characterized. The typical TEM image of $NiCo_2O_4$/$Ni(OH)_2$ composite is shown in Fig. 2(a) (the large area of TEM image are shown in Fig .S1), it is clearly that the products are hexangular nanosheets with an average diameter size of 200-300 nm and nanoparticles with an average size of 15-30 nm. It is worth noting that the nanoparticles are all adhere tightly to the hexangular nanosheets. The morphologies of the composite are influenced by the calcination temperature as shown in Fig. 2 (d-f). From the TEM images we know that the composite obtained at 350 ℃ had appropriate pore size, relative complete structure. The SEM and TEM images of the $NiCo_2O_4$/NiO composite (350 ℃) are shown in Fig. 2 (b, c) and Fig. 2 (g), respectively. We can clearly see that among the composite, hexangular ring-core porous $NiCo_2O_4$ nanosheets with a size range of 200-300 nm, the core size is about 130 nm and the ring with a width of 50 nm, the NiO nanoparticles with an average size of 15-30 nm. It is a remarkable fact that the ring of the hexangular ring-core structures is porous and the pore size is approximately 3 nm and consistent with the result of the pore size distribution curves as shown in Fig. 4 (a).

The HRTEM images of the magnified images marked with the large red rectangle and small red rectangle in Fig. 2 (g) give clear lattice fringes with spacings about 0.285 nm and 0.248 nm (Fig. 2 h), corresponding to (220) and (311) planes of $NiCo_2O_4$, which are consistent with the result of XRD pattern shown in Fig. 1 (b). Similarly, the lattice fringes with its spacings about 0.244 nm and 0.211 nm (Fig. 2i) could be attributed to (111) and (200) planes of NiO. Elemental mappings of the composite in Fig. 2 (j) show the uniform distribution of Ni, Co and O elements. In addition, the EDS (Fig. S2) and ICP-AES analysis (Table S3) of the composite (350 ℃) show that the molar ratio of $NiCo_2O_4$ and NiO are ~1:1.

The discharge-charge curves in the cycles of the hexangular ring-core porous $NiCo_2O_4$ nanosheets/NiO nanoparticles composite (350 ℃) at a current density of 100 mA g^{-1} were displayed in Fig. 3 (a), the composite in this study delivered a high first discharge and charge capacities of 1920.6 and 1435.3 mA h g^{-1}, resulting a coulombic efficiency of 74.73 % and the irreversible capacity of the first cycle may be attributed to the irreversible reactions related to the formation of SEI film[19] and incomplete oxidation of Ni, Co. The coulombic efficiency increased to 95% for the next cycles and the specific capacity maintained at 1567.3 mA h g^{-1} after 50 cycles (Fig.

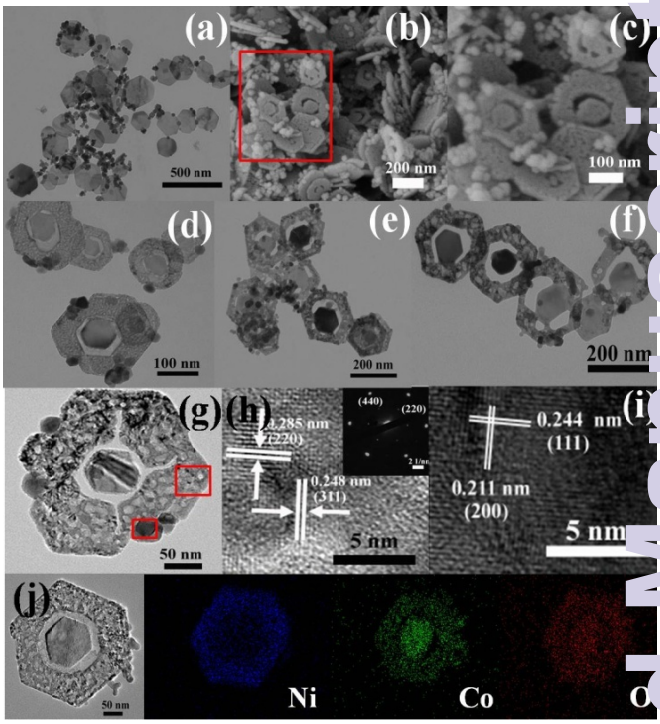

Fig. 2 TEM image of the $NiCo_2O_4$/$Ni(OH)_2$ (a); TEM images of composi obtained at different calcination temperatures (d) 300 ℃, (e) 400 ℃, (f) 500 SEM (b, c) and HRTEM (g, h, i) images of $NiCo_2O_4$/NiO (350 ℃) elemental mappings of the products after calcinations (j);

3b), indicating a good reversibility of the electrode. Fig. 3 (showed that at the current density of 200 mA g^{-1}, the first discharg and charge capacities are 1281.2 mA h g^{-1} and 971.2 mA h g^{-1} resulting in a coulombic efficiency of 75.8 % and the specif capacity maintained at 894 mA h g^{-1} after 200 cycles as shown in Fig. 3 (d). At the current density of 500 and 1000 mA g^{-1}, they showed high reversible capacity of 893 mA h g^{-1} after 455 cycles and 75 mA h g^{-1} after 740 cycles as shown in Fig. 3 (g, h). The phenomen of the capacity increasing with cycling has been found in ma transition metal oxides anode materials.[20, 21] In this study, it might be attributed to the decomposition of the electrolyte and struc variations of the composite after long cycling. Although th performance is still should be further improved, it is already better than those of the related reports (Table S1). In addition, the electrochemical performance of the working electrodes whi consist of active materials (70 wt. %), carbon black (20 wt. %), a carboxymethyl cellulose (CMC) (10 wt. %) were shown in Fig. S the comparion between carbon black content were 20 wt. % and 30 wt. % showed that the carbon black could increase the stability the material. $NiCo_2O_4$ nanosheet/$Ni(OH)_2$ nanoparticle composi showed good electrochemical performances which were shown Fig. S3 (see ESI†). Electrochemical impedance measurements were carried out for the coin cell containing the $NiCo_2O_4$/NiO composi electrode before and after 10th cycling at the current density of 50 mA g^{-1} as shown in Fig. S5. The semicircle area in the high frequency region was related to the charge transfer resistance (ct) in the electrode and electrolyte interface. In particular, the diam of the semicircle decreased after discharge-charge cycling for 10 cycles, this decrease in charge transfer resistance could be attribute to more electron and Li-ion transfer in the interface of the acti material and electrolyte, which result in the enhanced cyclin performance of the composite. The rate performance of th composite was showed in Fig. 3 (f). At the current densities of 10 200, 500, 1000 mA g^{-1}, the discharge specific capacities were 1884.6, 1168.9, 1111.2 and 1082.8 mA h g^{-1}, when the current densi returned to 100 mA g^{-1}, the specific capacity recovered to ~ 1439.7

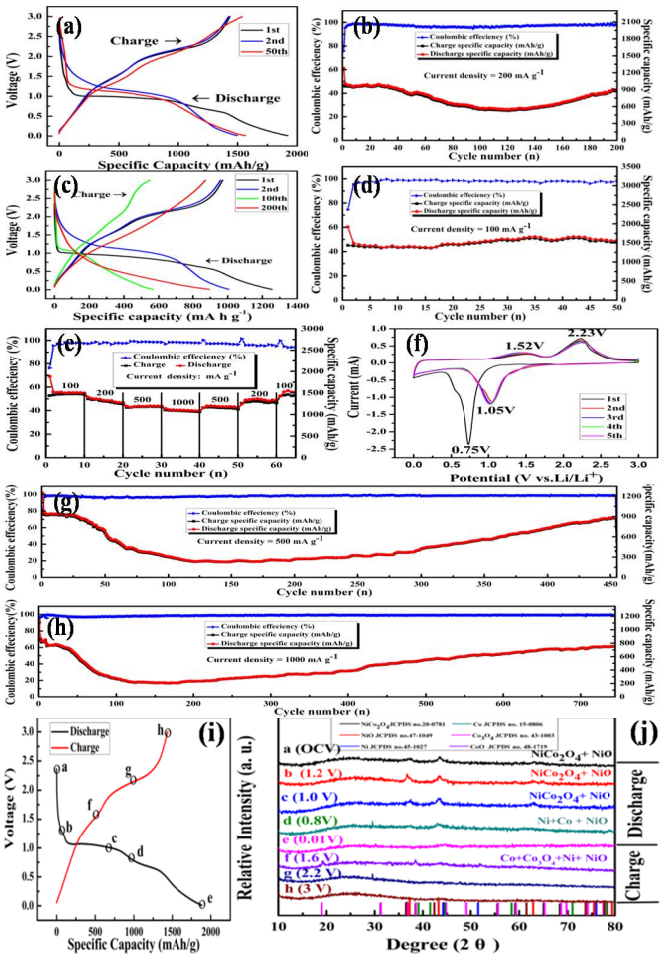

Fig. 3 Electrochemical properties of the composite (350 □). The charge-discharge curves at 100 mA g^{-1} (a) and 200 mA g^{-1} (c); Cycling performance and coulombic efficiency (b, d, g, h); CV curves (f) and rate performance (e); (i) The discharge/charge curves of the first cycle (100 mA g^{-1}) ; (j) Ex-situ X-ray diffraction patterns collected at various charge and discharge states.

mA h g^{-1} indicating good cycle stability of the electrode material. In addition, TEM images of the cycled composite at a current density of 100 mAg^{-1} after 50 cycles were shown in Fig. S6, the structure of the composite was relatively complete, which also indicated good stability of the electrode material. The enhanced electrochemical performances of $NiCo_2O_4$/NiO composite might be attributed to their unique structure features. The hexangular ring-core structure could increase the volume and surface area ratio and buffer the volume changes, meanwhile, the porous structure could allow electrolyte to diffuse into active materials easily, increase the contact between electrolyte and active material, and shorten the transport length of Li^+ ions. On the other hand, the synergetic effect of NiO nanoparticles and porous hexangular ring-core $NiCo_2O_4$ is responsible for the enhanced electrochemical performance of $NiCo_2O_4$/NiO composite. Moreover, the composites obtained at different temperatures (300 □, 400 □, 500 □) as anode materials have been tested (Fig. S7), the results showed that the composite obtained at 350 □ with appropriate pore size and relative complete structure has better electrochemical performance than other composites.

Fig. 3(f) shows the cyclic voltammograms of the $NiCo_2O_4$/NiO composite for the 1st, 2nd, 3st, 4th and 5th cycles at a scan rate of 0.1 mV s^{-1} in the voltage window of 0.01–3 V Li/Li^+. During the first reduction scan, an intense reduction peak around 0.75V was observed, which might be assigned to the reduction of $NiCo_2O_4$ to metallic Ni and Co (Eqs.1). Meanwhile, the two oxidation peaks at around 1.5 V and 2.2 V correspond to the oxidation of Ni^0 to Ni^+ (Eqs. 2) and Co to Co^{3+} (Eqs. 3 and 4). During the subsequently cycles, the reduction peak shifted to around 1.05 V and the oxidation peaks changed inconspicuous. The CV curves were similar after the first cycle, which suggested that the performance of the electrode is stable. The lithium intercalation and extraction in reactions might be attributed to process as follows: [6, 22]

$$NiCo_2O_4 + 8Li^+ + 8e^- \rightarrow Ni + 2Co + 4Li_2O \quad (1)$$

$$Ni + Li_2O \leftrightarrow NiO + 2Li^+ + 2e^- \quad (2)$$

$$Co + Li_2O \leftrightarrow CoO + 2Li^+ + 2e^- \quad (3)$$

$$CoO + 4/3Li_2O \leftrightarrow 1/3Co_3O_4 + 8/3Li^+ + 8/3e^- \quad (4)$$

In addition, we have investigated the charge-discharge mechanism of the composite as anode for LIBs by the combination of electrochemical measurement and the Ex-situ XRD analysis. A series of partially lithiated cells were selected at different voltage states, see the letters ''a'' to ''h'' denoted in Fig. 3 (i), and the corresponding Ex-situ X-ray patterns are shown in Fig. 3 (j). During the first discharge process from OCV to 0.01 V, the XRD patterns of the electrode that discharged to 1.2 V (a) and 1.0 V (b) have similar characteristics as that of the fresh electrode ($NiCo_2O_4$/NiO), revealing there are no obvious electrochemical reaction has been initiated till 1.0 V (c). When the electrode was discharged to 0.8 V (d), the peak intensity of these XRD patterns were obviously weaken and the diffraction peak of Ni and Co appeared, which are consistent with that of the cyclic voltammograms data (see Fig. 3e) where the intense reduction peak sets in ~0.75 V. In addition, we could not observe any obvious diffraction peaks that corresponding to metallic Co and Ni in the XRD pattern when the electrode was discharged to 0.01 V (e), which might be attributed to the nanoparticle nature of the electrochemically formed species. During the charge process from 0.01 V to 3 V, when electrode was charged to 1.6 V, the diffraction peaks in the XRD patterns (NiO, CoO and Co_3O_4) are consistent with the process (2, 3, and 4). Similarly, when the electrode was charged to 2.2 V (g) and 3.0 V(h), no obvious diffraction peakswere observed, indicating the formation of amorphous oxides during the charge process, this phenomenon is similar with that of the previ-ous report.[23] Through these analysis, we could preliminary confirm the charge-discharge mechanism of the composite for LIBs.

Fig. 4 (a) showed nitrogen adsorption /desorption isotherm and the corresponding pore size distribution curve (inset) of the composite (350 □). It gives an obvious hysteresis loop of type IV which is the character of microsporous materials. The surface area and pore volume of the composite are 78.51 m^2 g^{-1} and 0.074 cm^3 g^{-1}, which are favourable for the composite as catalysts for CO oxidation. Fig. 4 (b) presents the catalytic activities of the composites as function of reaction temperature (300 □, 350 □, 400 □, 500 □). It is clearly that the composite obtained at 350 □ showed better catalytic activity. For the composite (350□), along with the increasing temperature, the CO conversion increases slowly at first and then rises sharply at 77 ℃ and complete CO conversions can be achieved at 115 ℃. The catalytic stability towards CO oxidation are further investigated and it can be seen from the CO conversion rate versus time on stream curves (Fig. 4 c) that the catalysts demonstrate good stability with almost no changes relative in the 75% CO conversions after 120 min on stream and the temperatures for the catalytic life tests are 108 □ respectively. The H_2-temperature programmed reduction (H_2-TPR) profile of $NiCo_2O_4$/NiO catalyst (Fig. 4d) shows that the composite

has lower reduction temperature of Ni^{2+}, Co^{3+}, Co^{2+} than the previously reported individual $NiCo_2O_4$ (Co^{3+} to Co^{2+}, 315 ℃; Co^{2+}

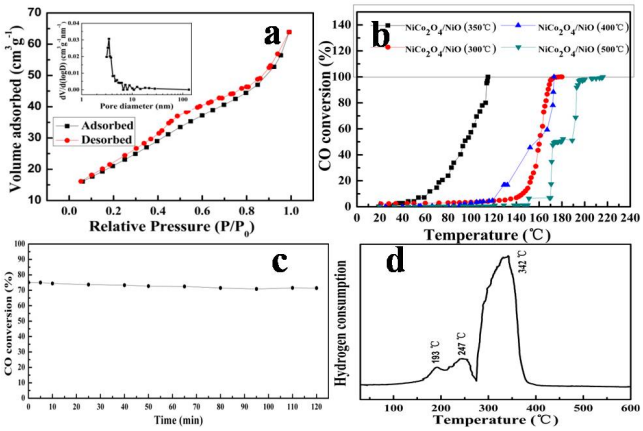

Fig. 4 (a) Nitrogen adsorption /desorption isotherm and the corresponding pore size distribution (inset) (350 □); (b) Percentage conversion of CO as a function of reaction temperature of the composites obtained at different temperatures; (c) CO conversion versus time on stream plots; (d) The H_2-Temperature-programmed reduction (H_2-TPR) profile of the composite.

to Co, 367 ℃ and Ni^{2+} to Ni, 257 ℃) [24] and individual NiO (Ni^{2+} to Ni, ~360 ℃), [25] the lower reduction temperature of the composite might be mainly attributed to the synergistic effect of the two components. In the composite, $NiCo_2O_4$ belongs to cubic system and isostructural to Co_3O_4 with spinel structure. According to the previous reports,[26, 27] Co^{3+} is the active site of the CO oxidation, large amounts of Co^{3+} cations provide sufficient sites for CO adsorption, which occurs easily. The reaction between the adsorbed CO and the nearby active oxygen species to form CO_2 might be the rate-determining step. Similarly, NiO belongs to cubic system, Ni^{2+} is the active site of the CO oxidation according to the previous report, [28] and the CO adsorbed to Ni-O reacting with the active oxygen species to form CO_2. In addition, the results of the TEM images (Fig. S8) and XRD pattern (Fig. S9) of the $NiCo_2O_4$/NiO catalyst after CO oxidation reaction reveal the relative high stability of the composite. The preliminary catalytic data show that the $NiCo_2O_4$/NiO catalyst exhibits enhanced activity and good stability toward CO oxidation, which might be attribute to the porous ring-core structural $NiCo_2O_4$ with sufficient area surface for the adsorbing of gases and the NiO nanoparticles with small size (15-30 nm) for decreasing of inner diffusion resistance. Therefore, the $NiCo_2O_4$/NiO composite is promising as catalytically active material in heterogeneous catalysis.

In summary, hexangular ring-core $NiCo_2O_4$ porous nanosheets /NiO nanoparticles are successfully synthesized through a facile hydrothermal reaction followed by a calcinations process. The as-obtained composite as anode material exhibits a high initial discharge capacity of 1920.6 mA h g^{-1} at a current density of 100 mA g^{-1} and the capacity is retained at 1567.3 mA h g^{-1} after 50 cycles. The enhanced electrochemical capability could be ascribed to the unique porous hexangular ring-core structure and the synergetic effect of NiO nanoparticles and porous hexangular ring-core $NiCo_2O_4$. At the same time, the CO oxidation catalytic activity of the composite are tested, and complete CO conversions is achieved at 115 □. The catalyst demonstrates good stability with almost no changes relative in the 75% CO conversions after 120 min on stream and the temperatures for the catalytic life tests are 108 □, respectively. Accordingly, the hexangular ring-core $NiCo_2O_4$ porous nanosheet/NiO nanopaticle composite is promising as anode material for LIBs and catalyst for CO oxidation catalytically.

Acknowledgements

This research was financially supported by the 973 Project of China (no. 2011CB935901), National Science Foundation of China and Academy of Sciences large apparatus United Fund (no. 21471091 and 11179043) and the Fundamental Research Funds of Shandong University (no. 2015JC007).

Notes and references

[a] Key Laboratory of Colloid and Interface Chemistry, Ministry of Education School of Chemistry and Chemical Engineering, Shandong University, Jinan, 250100, P.R. China. E-mail: Xulq@sdu.edu.cn

† Electronic Supplementary Information (ESI) available: TEM images and cycling performances of the product obtained after the hydrothermal reaction; electrochemical impedance spectra for composite cell before and after discharge–charge; Comparisons between the $NiCo_2O_4$/NiO composite and previously reported related nanocomposite; Cycling performances of the products obtained at different temperature; The TEM images and XRD pattern of the composite after CO oxidation reaction; Comparisons between the composite and previously reported anode materials; the ICP analysis of the composite. See DOI: 10.1039/c000000x/

1 Z. S. Wu, W. C. Ren, L. Wen and L. B. Gao, *ACS Nano*, 2010, **4**, 3187.
2 Z. Z. Bai, Z, C, Ju, C. L. Guo, Y. T. Qian, B. Tang and S. L. Xiong, *Nanoscale*, 2014, **6**, 3268.
3 Y. J. Zhai, X. J. Ma, H. Z. Mao, W. W. Shao, L.Q. Xu, Y. Y. He, and Y. T. Qian，*Adv. Electron. Mater.*，2015，1400057.
4 L. Hu, N. Yan, Q. W. Chen, P. Zhang, H. Zhong, X. R. Zheng, Y. Li and X. Y. Hu, *Chem. Eur. J.*, 2012, **18**, 8971.
5 X. Xie, Y. Li, Z. Q. Liu, H. Masatake and W. J. Shen, *Nature* 2009, **458**, 746.
6 Y. J. Zhai, H. Z. Mao, P. Liu, X. C. Ren, L.Q. Xu and Y. T. Qian, *J. Mater. Chem. A*, 2015, DOI: 10.1039/C5TA03017J .
7 Y. Sharma, N. Sharma, G. V. S. Rao and B.V.R. Chowdari, *J. Power Sources,* 2007, **173**, 495.
8 G. D. Li, L. Q. Xu, Y, J, Zhai and Y. P. Hou, *J. Mater. Chem. A,* 2015, **3**, 14298.
9 Y. G. Li, P. Hasin and Y. Y. Wu, *Adv. Mater*., 2010, **22**, 1926.
10 G. Huang, L. L. Zhang, F. F.Zhang and L. M. Wang, *Nanoscale*, 2014, **6**, 5509.
11 G. Y. Zhang, B. Guo and J. Chen, *Sens. Actuators, B,* 2006, **114**, 402.
12 J. K. Zhu and Q. M. Gao, *Microporous Mesoporous Mater*., 2009, **124**, 144.
13 Y. Gou, X. Lian and B. H. Chen, *J. Alloys Compd*., 2013, **574**, 181.
14 Y. C. Dong, C. W. Cao, Y. S. Chui, J. A. Zapien, *Chem. Commun.*, 2014, **50**, 10151.
15 D. Zhou, X. R. Su, M. Boese, R. M. Wang, H. Z. Zhang, *Nano Energy*, 2014, **5**, 52.
16 Y. J. Chen, M. Zhuo, J. W. Deng, Z. Xu, Q. H. Li and T. H. Wang, *J. Mater. Chem. A*, 2014, **2**, 4449.
17 B. Cui, H. Lin, J. B. Li, X. Li, J. Yang and J. Tao, *J. Mater. Chem.*, 2009, **113**, 14083.
18 B. Cui, H. Lin, Y. Z. Liu, J. B. Li, P. Sun, X. C. Zhao and C. J. Liu, *Adv. Funct. Mater.*, 2008, **18**,1440.
19 N. Munichandraiah, L. G. Scanlon and R. A. Marsh, *J. Power Sources*, 1998, **72**, 203.
20 J. Y. Shin, D. Samuelis and J. Maier, *Adv. Funct. Mater.*, 2011, **21**, 3464.
21 R. R. Zhang, Y. Y. He and L. Q. Xu, *J. Mater. Chem. A*, 2014, **2**, 17779.
22 H. S. Jadhav, R. S. Kalubarme, C. N. Park, J. Kim and C. J. Park, *Nanoscale*, 2014, **6**, 10071.
23 Y. Sharma, N. Sharma, G. V. S. Rao and B. V. R. Chowdari, *Adv. Funct. Mater.,* 2007, **17**, 2855.
24 D. G. Klissurski and E. L. Uzunova, *Chem. Muter.* 1991, **3**, 1060.
25 N. K. Kotsev and L. I. Ilieva, *Catal. Lett.* .1993, **18**, 173.
26 J. Jansson, *J. Catal.*, 2000, **194**, 55.
27 X. Xie, Y. Li, Z. Q. Liu, H. Masatake and W. J. Shen, *Nat.*, 2009, **458**, 746.
28 C. J. Tang, J. C. Li, X. J. Yao, J. F. Sun, Y. Cao, L. Zhang, F. Gao, C. Deng and L. Dong, *Appl. Catal., A,* 2015, **494**, 77.